mathematics

MDPI

Article

Mesh Free Radial Point Interpolation Based Displacement Recovery Techniques for Elastic Finite Element Analysis

Mohd. Ahmed [1,*], Devinder Singh [2], Saeed AlQadhi [1] and Majed A. Alrefae [3]

[1] Civil Engineering Department, College of Engineering, King Khalid University, Abha 61421, Saudi Arabia; sdalqadi@kku.edu.sa
[2] State Insurance Corporation, New Delhi 110077, India; dr_dsingh@hotmail.com
[3] Mechanical Engineering Department, Royal Commission of Jubail & Yanbu, Yanbu 41912, Saudi Arabia; refaem@rcyci.edu.sa
* Correspondence: mall@kku.edu.sa; Tel.: +966-172-418-439

Abstract: The study develops the displacement error recovery method in a mesh free environment for the finite element solution employing the radial point interpolation (RPI) technique. The RPI technique uses the radial basis functions (RBF), along with polynomials basis functions to interpolate the displacement fields in a node patch and recovers the error in displacement field. The global and local errors are quantified in both energy and L_2 norms from the post-processed displacement field. The RPI technique considers multi-quadrics/gaussian/thin plate splint RBF in combination with linear basis function for displacement error recovery analysis. The elastic plate examples are analyzed to demonstrate the error convergence and effectivity of the RPI displacement recovery procedures employing mesh free and mesh dependent patches. The performance of a RPI-based error estimators is also compared with the mesh dependent least square based error estimator. The triangular and quadrilateral elements are used for the discretization of plates domains. It is verified that RBF with their shape parameters, choice of elements, and errors norms influence considerably on the RPI-based displacement error recovery of finite element solution. The numerical results show that the mesh free RPI-based displacement recovery technique is more effective and achieve target accuracy in adaptive analysis with the smaller number of elements as compared to mesh dependent RPI and mesh dependent least square. It is also concluded that proposed mesh free recovery technique may prove to be most suitable for error recovery and adaptive analysis of problems dealing with large domain changes and domain discontinuities.

Keywords: error estimation; effectivity; basis function; meshfree recovery technique; radial point interpolation; radial basis function

Citation: Ahmed, M.; Singh, D.; AlQadhi, S.; Alrefae, M.A. Mesh Free Radial Point Interpolation Based Displacement Recovery Techniques for Elastic Finite Element Analysis. *Mathematics* **2021**, *9*, 1900. https://doi.org/10.3390/math9161900

Academic Editor: Basil Papadopoulos

Received: 9 July 2021
Accepted: 3 August 2021
Published: 10 August 2021

1. Introduction

The finite element method (FEM) has become a widely accepted method for the solution of solid mechanics problems. However, the error in finite element solutions is introduced by the very process of discretization of the problem domain. The causes of errors include error due to approximation made during mathematical modeling of the physical situation, error due to rounding off, and error due to discretization. The discretization error connected with the finite element mesh can be controlled with the choice of the type and size of elements. The discretization errors are introduced when the displacement interpolation polynomial does not accurately represent the behavior of the continuum. The current research developments in the finite element method include the improvement of the accuracy, effectivity, and reliability of FEM results of industrial problems [1]. The recent developments in high-performance finite element methods are reviewed by Cen et al. [2]. In the recovery-based error estimation, the difference between the values of recovered more accurate displacements/stress and displacements/stress obtained by the finite element solution provides a measure of the local error. The point-wise definitions

are not only difficult to estimate and become meaningless at singularities. Therefore, alternative scale measures or norms are preferable. A particularly useful one is given by the energy norm, which represents the error in the rate of energy dissipation. The error norms of the displacements, such as the L_2 norm, representing straightforward physical meaning, show for many finite elements super-convergence properties [3]. Zienkiewicz and Zhu [4] presented a local projection technique, a super convergent patch recovery technique, to recover the errors in stresses using the least square fit of the local polynomial to the super convergent value of the derivatives over node patch. The post-processing technique to recover the stresses and displacements from the finite element solution is presented by Niu and Shephard [5]. The error post-processing technique for displacements in the L_2 norm is due to Li and Wiberg [6]. The recovery by equilibrium and compatibility in patches is proposed by Ubertini [7] to recover the error in the FEM solution for stresses. The traditional recovery techniques use the least square fitting of displacement/stress over the mesh dependent patches. The mesh free methods are recently introduced for recovery of FEM solutions errors through various mesh free support domains based interpolating techniques. The mesh free approaches are developed for situations in which distortion of elements occurs due to large domain changes and domain discontinuities. A coupled element-free Galerkin method (EFG) Method and finite element method (FEM) error recovery procedure based on local maximum entropy shape functions, for material and geometrical nonlinearities problems, is proposed by Ullah et al. [8]. The Chung and Belytschko [9] error estimations are used in the EFG regions and Zienkiewicz and Zhu (ZZ) super convergent patch recovery is used for strains and stresses in the FE region of the problem domain.

Nadal et al. [10] propose the explicit-type recovery error estimator in energy norm for the linear elasticity problem using a smooth solution. The discontinuous Galerkin error estimator-based hp-adaptive finite element analyses were carried out by Bird et al. [11]. The performances of the hp-adaptive scheme are compared with uniform and h-refinement adaptive scheme achieving the exponential rates of convergence. Liu et al. [12] propose a linear conforming point interpolation methodology-based meshfree Galerkin method for two-dimensional solid mechanics problems. Liu and Zhang [13] have proposed a strain-constructed point interpolation method (SC-PIM) for the analysis of static, free, and forced vibration structures problems. A thorough analysis of error estimation considering moving least square interpolation is presented by Mirzaei [14]. The study of factors affecting the accuracy and reliability of smoothed radial point interpolation method (RPIM) is carried out by Hamrani et al. [15]. A hybrid approach based on smoothed radial point interpolation method (CS-RPIM) and FEM is proposed by Zhang et al. [16] for solving fracture problems. Cao et al. [17] proposed a hybrid mesh free Galerkin RPIM and FEM to impose the essential boundary conditions. The mesh free recovery method using support domains, i.e., zone of influence of a node, was recently introduced by Ahmed et al. [18] to recover the FEM solution errors. The comparison of error estimation behavior using meshfree methods, RPI error recovery method, and MLS interpolation, and mesh dependent ZZ recovery method was presented by Ahmed [19] and concluded that the quality of error estimation of meshfree recovery methods was better than the mesh dependent error recovery methods. A two-dimensional finite element model employing mesh free nodes interface model based radial point interpolation method to simulate the interaction between soil and structure is proposed by Gong et al. [20].

From the literature review, it is evident that most of the techniques proposed to recover the discretization error introduced in the finite element solution are mesh-based, i.e., dependent on element mesh connectivity, and the mesh free recovery technique in finite element method is a recent interest. The existing mesh-based techniques may not perform well or are difficult to implement in situations to deal with large domain changes and domain discontinuities. Moreover, more attention has been paid to recover errors in the field variable derivatives. Therefore, there is a need to develop mesh free recovery techniques using the different mesh free procedures with special attention to recover errors

in the field variable. The present study aimed to investigate the reliability and effectiveness of RPIM-based displacement error recovery techniques in the mesh free environment. The comparison of mesh free RPIM-based displacement error recovery techniques with mesh dependent RPIM and least square based recovery techniques is also carried out. The study also compares the performance of RPI-based error recovery techniques with Zienkiewicz-Zhu (ZZ) recovery techniques presented in the literature [18]. The benchmark elastic plates examples are analyzed to compare the rate of error convergence, effectivity, and adaptively improved meshes with different displacement recovery procedures. The linear triangular, quadratic triangular, and quadrilateral elements are used for problems domain discretization. The errors of finite element solution are computed directly from the recovered displacement in terms of energy and L_2 norm. The influence of radial basis functions in RPI-based recovery techniques is also assessed by considering three radial basis functions, namely multi-quadrics, gaussian (exponential), and thin plate splint for the RPI technique. The effect of radial basis functions with their shape parameters and shape of node zones is also assessed on the quality of the error estimation obtained from the RPI-based error recovery techniques.

2. Elastic Problem Statement

The elastic problems are considered with stress field, "σ" and unknown displacement field "$\boldsymbol{u}$", defined over a domain Ω that is bounded by $\Gamma = \Gamma_t \cup \Gamma_u$. The prescribed tractions ($\bar{t}$) and displacements ($\overline{u}$) are imposed over boundary Γ_t and Γ_u, respectively.

The equilibrium conditions and boundary conditions are satisfied to find ($\boldsymbol{\sigma}$,$\boldsymbol{u}$).

$$L^T \boldsymbol{\sigma} + \boldsymbol{f} = 0 \text{ in } \Omega, \tag{1}$$

where $\boldsymbol{f}$ is the force vector, L^T is the derivative operator.

$$\boldsymbol{\sigma} \cdot \boldsymbol{n} = \bar{t} \text{ on } \Gamma_t, \tag{2}$$

$$\boldsymbol{u} = \overline{u} \text{ on } \Gamma_u, \tag{3}$$

Constitutive relation:

$$\boldsymbol{\sigma} = \boldsymbol{D}\, \boldsymbol{\varepsilon}, \text{ with } \boldsymbol{\varepsilon} = L\, \boldsymbol{u}, \tag{4}$$

where $\boldsymbol{D}$ is the elasticity matrix of linear isotropic material and ε is the strain vector.

3. Least Square Interpolation Technique for Displacement Recovery

The recovery of field variable (displacement) is obtained by least squares fit of the computed nodal field variable using a higher order polynomial over an element neighborhood patch consists of a union of the elements surrounding an element. To perform least square fitting, the following functional is minimized.

$$\pi_f\,(a) = 1/2 \sum_{i=1}^{np} [d_i^h(x_i, y_i) - d_i\,(x_i, y_i)]^2 \tag{5}$$

where $\boldsymbol{u_i}\,(x_i, y_i) = \boldsymbol{P_i}\,(x_i, y_i)\,.\,\boldsymbol{a}$

$$\boldsymbol{u_i} = [u_i\ v_i\ ]^T\ ,\ \boldsymbol{a} = [a_u\ a_v\ ]^T \tag{6}$$

where u_i and v_i are the nodal parameters of field variables in x and y direction and **a** is the vector of unknown parameters a_u and a_v.

$$\mathbf{p_i} = [1, x_i, y_i, x_i^2, x_i y_i, y_i^2, \ldots\ldots], \tag{7}$$

where (x_i, y_i) are the sampling points (np) coordinates.

Minimization condition of $\pi_f\,(a)$ implies that "$\boldsymbol{a}$" satisfies the following relation.

$$\sum_{i=1}^{np} P_i^{\,T}(x_i, y_i).\ P_i\,(x_i, y_i).\ a = \sum_{i=1}^{np} P_i^{\,T}(x_i, y_i).\ d_i^{\,h}(x_i, y_i) \tag{8}$$

Solving for "a", the following relation is obtained.

$$\boldsymbol{a = A^{-1}\, b}, \tag{9}$$

where

$$\mathrm{A} = \sum_{\mathrm{i}=1}^{\mathrm{np}} P_i{}^T(x_i, y_i).\ P_i\,(x_i, y_i).a, \text{ and } b = \sum_{i=1}^{np} P_i{}^T(x_i, y_i).\ d_i{}^h(x_i, y_i) \tag{10}$$

4. Radial Point Interpolation Method (RPIM) for Displacement Recovery

The radial point interpolation method (RPIM) considers both the radial basis functions (RBF) and polynomials basis function for interpolation [21]. The approximation $u^h(x)$ for the field variables $u(x)$ at a point x_q, assuming only the influencing nodes of a point x_q have an effect on $u(x)$, is given by,

$$u^h\,(x, x_q) = \sum_{\mathrm{i}=1}^{\mathrm{n}} R_i\, a_i + \sum_{\mathrm{j}=1}^{\mathrm{m}} p_j\, b_i = R^T(x)\, a + p^T(x)\, b, \tag{11}$$

where R_i is the RBF computed at x_i, the ith node in the support domain of x_q, p_j is the monomial in the polynomial basis, a_i and b_j are the coefficient for the radial basis function (R_i) and polynomial basis (p_j) respectively, n is the number of nodes in the mesh free nodes zones of x_q, m is the number of monomials in the polynomial basis.

$$a = [a_1, a_2, \ldots, \ldots \ldots ..a_n] \tag{12}$$

$$b = [b_1, b_2, \ldots, \ldots \ldots ..b_n] \tag{13}$$

$$R(x) = [R_1(x), R_2(x), \ldots \ldots, \ldots \ldots\ R_n(x)]^T, \tag{14}$$

$$p(x) = [p_1(x), p_2(x), \ldots \ldots, \ldots \ldots\ p_n(x)]^T, \tag{15}$$

the text following an equation need not be a new paragraph. Please punctuate equations

The number of the radial basis 'n' and the order of polynomial basis 'm' is chosen based on the reproduction requirement. Minimum terms of polynomial basis are often adopted for better stability. The coefficients a_i, and b_j are determined in this way such that Equation (12) passes through 'n' data nodes in the mesh free nodes zones and imposing constraints on the polynomial basis functions to guarantee a unique solution [22]. Thus, two intermediate matrices S_a and S_b result as follows,

$$R_b = [P_m{}^T\, R_q{}^{-1}\, R_i]^{-1}\, P_m{}^T\, R_q{}^{-1}, \tag{16}$$

$$R_a = P_m{}^T - R_q{}^{-1}\, P_m\, S_b, \tag{17}$$

where R_q is the moment matrix associated to the radial basis function and P_m is the moment matrix related to the polynomial terms. The solution of Equation (12) is only possible if the number of unknown parameters a is smaller than, or at the most equal to, the number of independent equations.

The 'n' number of equations can be obtained using Equations (11), (16) and (17) as,

$$u^h = R_q\, a + P_m\, b, \tag{18}$$

The following constraints are imposed to obtain unique solutions of the equation,

$$p_m{}^T\, a = 0, \tag{19}$$

Combining Equations (18) and (19) yields.

$$a = S_a\, u^e, \tag{20}$$

$$b = S_b\, u^e, \tag{21}$$

Substituting the Equations (20) and (21) into Equation (18), the interpolation function ψ(x) can be obtained as.

$$u^h(x, x_q) = (R^T S_a - p^T S_b) u^e = \psi(x) u^e, \quad (22)$$

4.1. Multi-Quadrics Radial Function (MQ)

The radial basis function performs an influential role on the behavior of RPI methods. The various types of radial basis functions can be used for RPI technique. The formulation of multi quadrics (MQ) radial basis function with dimensionless shape parameters is as follows.

$$R_i(x_j) = [(x_j - x_i)^2 + (y_j - y_i)^2 + (\alpha_0\_d_c)^2]^q, \ \alpha_0 \geq 0 \quad (23)$$

where α_0 is a dimensionless coefficient and d_c represents characteristic length that relates to the nodal spacing in meshfree nodes zones or nodes patch of the point of interest x, which is the shortest distance between the node i and neighborhood nodes.

4.2. Gaussian (Exponential) Radial Basis Function (Exp)

The formulation of Gaussian (Exponential) radial basis function with dimensionless shape parameters is as follows.

$$R_i(x_j) = exp\{-\alpha_0 [(x_j - x_i)^2 + (y_j - y_i)^2 / {d_c}^2]\}, \quad (24)$$

4.3. Thin Plate Splint (TPS) Radial Basis Function (Exp)

The formulation of thin plate splint (TPS) radial basis function is as follows.

$$R_i(x_j) = \{\sqrt{[(x_j - x_i)^2 + (y_j - y_i)^2]}\}^q, \quad (25)$$

The α_0, q and η are the shape parameters of the RBFs. In utilizing RBFs, the shape parameters need to be determined for good performance. Effects of α_0 and q on radial basis functions have been widely investigated [23]. It was found that for 2D square plate problem using MQ radial basis function and errors quantified in energy norm, $\alpha_0 = 5.0$ and $q = 1.03$ lead to good results while α_0 should be less 1 for Gaussian RBF. Hence, these values were used in the study. However, for L_2 norm, $\alpha_0 = 1$ and q should be less than 0.5 for best performance with MQ. It was also observed that with increasing node zone size, the value of $\alpha 0$ should also be increased for the best performance of RPI-based recovery analysis. The value of $\alpha_0 = 0.65$ and $q = 1.03$ is taken in plate problem with opening for MQ RBF. The value of $\alpha_0 = 0.65$ is taken with Gaussian RBF and $\eta = 5$ is taken with TPS RBF for error quantified in the energy norm.

The second term in Equation (11) consists of polynomials. The linear polynomial added into the RBF can ensure linear consistency and improve interpolation accuracy [23]. The linear polynomial basis with m as 3 is used in the RPI technique, which is given as

$$p^{\mathrm{T}}(x_i) = [1, x_i, y_i,], \quad (26)$$

The accuracy of interpolation for the point of interest depends on the nodes in the mesh free nodes zones. The circular form of mesh free nodes zones is constructed using the distance $d = \|x - x_i\|/d_m$. The $(x - x_i)$ is the distance from node x to point x_i and d_m is the size of the influence domain of the point x_i, the support size of the ith node, d_{mi}, is computed by $d_{mi} = d_{max}\, c_i$, in which d_{max} is a scaling factor called as dilation parameter, the distance c_I is determined by searching for sufficient neighbor nodes distance. The dilation parameter (d_{max}) is taken as 3.0 in the present study. For the construction of the rectangular form of meshfree nodes zones, the distance along two cartesian directions are $r_x = \|x - x_i\|/d_{mx}$ and $r_x = \|y - y_i\|/d_{mx}$, where $d_{mx} = d_{max}\, c_{xi}$ and $d_{my} = d_{max}\, c_{yi}$. For uniformly distributed nodes, c_i is simply the distance between two neighboring nodes. For nonuniformly distributed nodes, c_i can be taken as an average nodal spacing in the support domain of x_i.

5. Measurement of Errors

The error in computed state variable or state variable derivative i.e., displacement (u) or stress (σ), (e_u* or e_σ*) is defined as the difference between the exact (or numerical) values of u (or σ) and respective computed values, u^h (or σ^h).

$$e_u = u^* - u^h, \tag{27}$$

$$e_\sigma = \sigma^* - \sigma^h, \tag{28}$$

The specification of local error in the above manner is generally not convenient and may be occasionally misleading. For this reason, 'norm' representing integral scalar quantities are introduced to measure the error. For example, the energy norm is evaluated by computing the strain energy contained in the difference between the discontinuous value σ^h and the recovered values σ*. The 'energy norm' for the error, also called as error estimator can be written as in Equation (29).

$$\|x - x_i\|_E = [\int_\Omega e_\sigma{}^{*T} D^{-1} e_\sigma{}^* d\Omega]^{0.5}, \tag{29}$$

where "D" is the elasticity matrix.

A more direct quantification measure is the so-called L_2 norm, which can be associated with the error in any quantity. For example, for the displacement u, the L_2 norm of the error is obtained as given in Equation (30).

$$\|x - x_i\|_{L2} = [\int_\Omega e^T e^* d\Omega]^{0.5}, \tag{30}$$

An estimator is asymptotically exact for a problem if the problem global and local (element) effectivity index (θ), i.e., ratio of estimated error and actual error, converges to one when the mesh size approaches to zero [24].

$$\theta = \|e\| / \|e_{ex}\|, \tag{31}$$

where $\|e_{ex}\|$ and $\|e\|$ are the actual error and the estimated error in the energy norm.

The accuracy (η) of a finite element solution may be defined as follows.

$$\eta = \|e^*\| / \|\sigma^*\|, \tag{32}$$

$$\|\sigma^*\|^2 = \|\sigma^h\|^2 + \|e\|_E{}^2, \tag{33}$$

$$\|\sigma^h\|^2 = \sum_{i=1}{}^n \|\sigma^h\|^2{}_i, \tag{34}$$

The solution is acceptable if $\eta \leq \eta_{allow}$ where η_{allow} is the allowable accuracy. If $\eta > \eta_{allow}$, modification of element size is needed.

A 2-dimensional finite element code is developed incorporating the above described mesh free/mesh dependent error recovery techniques and error estimators guided adaptive techniques. The program is run on intel core i7 with 2.6 GHz processor and 16 GB RAM to obtain the numerical results of the following plate problems analysis. The flow chart to show the adaptive finite element analysis using the error recovery techniques implementation is shown in Figure 1.

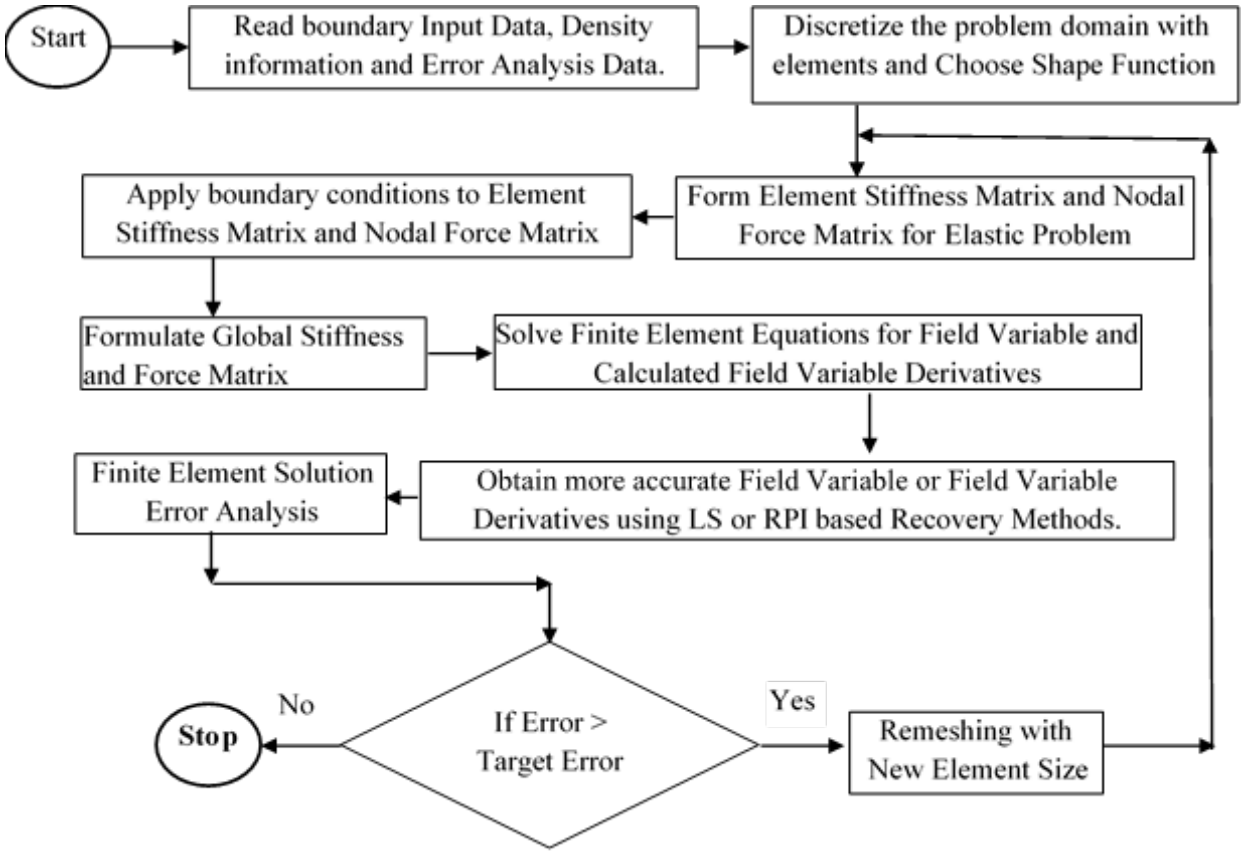

Figure 1. Least square and RPI recovery techniques coupled adaptive elastic finite element analysis flow chart.

6. Elastic Plate Problems

The quality of recovery method is obtained by adaptive finite element analysis of two elastic plate problems, for which analytical solution is available [4], in terms of error convergence rate, effectivity, and adaptive meshes employing above-discussed mesh free and mesh dependent recovery techniques. The problem domains are discretized with triangular (three nodes) and quadrilateral (four nodes) mesh. The RPI recovery-based analysis considers multi-quadrics radial basis function and quadratic polynomial basis function. The errors are quantified in both energy and L_2 norms. The mesh free nodes zones for RPI technique to interpolate the displacement/stress is shown in Figure 2. The least square and RPI approach uses the nodal values in the mesh dependent element patches consist of the union of the elements surrounding the element under consideration to interpolate the displacement/stress as shown in Figure 3.

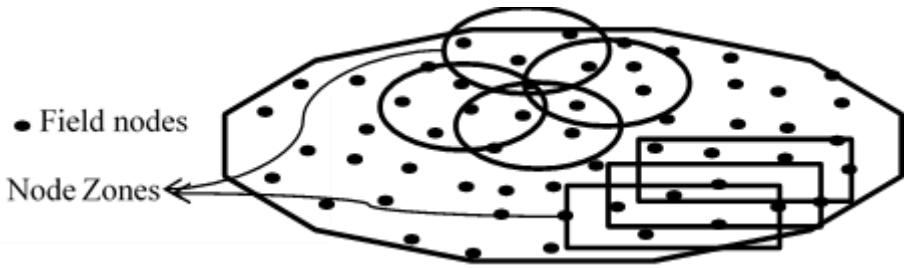

Figure 2. Mesh free node zones (Circular/Rectangular) for RPI bases recovery technique.

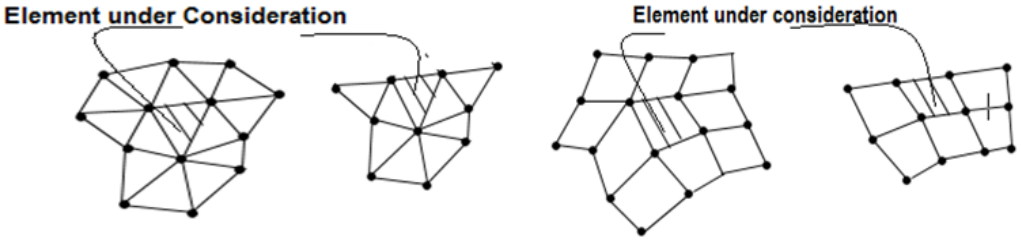

(**a**) Triangular Elements (**b**) Quadrilateral Elements

Figure 3. Element patches for least square (Displacement) and RPI (Displacement) recovery technique (mesh dependent).

6.1. Square Plate Problem

A 1 × 1 plane square plate problem was analyzed under the action of body forces (b_x, b_y) over the domain using various recovery techniques-based FEM in an adaptive environment. The body forces in the form of polynomials are given in Equations (35) and (36). The analytical solutions for displacements (u, v) are given in Equation (37). The discretized domain of the plate using triangular and quadrilateral elements is depicted in Figure 4. The analysis results for error convergence and effectivity for displacement recovery in different norms are tabled in Tables 1–6.

$$u = 0; v = -\mathrm{x}\,\mathrm{y}(1-\mathrm{x})\,\mathrm{x}\,(1-\mathrm{y}), \tag{35}$$

$$b_x = (\alpha + \beta)\,.\,(1-2\mathrm{x})\,.\,(1-2\mathrm{y}), \tag{36}$$

$$b_y = -2\,\beta\,\mathrm{y}.(1-\mathrm{y}) - (\alpha + 2\,\beta)\,2\mathrm{x}\,.(1-\mathrm{x}), \tag{37}$$

The constants α and β are given as

$$\alpha = \mathrm{E}\,\nu/[(1-2\nu)\,(1+\nu)];\ \beta = \mathrm{E}/[2(1+\nu)]$$

where E, ν are Modulus of elasticity and Poisson's ratio with a value of 1.0 N/mm^2 and 0.3.

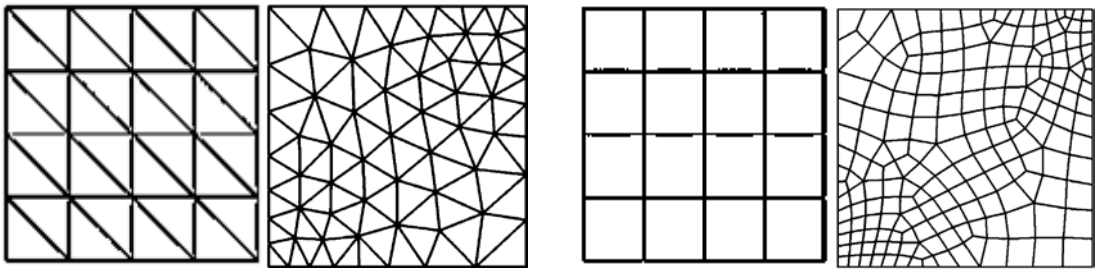

(**a**) Triangular Elements (**b**) Quadrilateral Elements

Figure 4. Subdivided elements mesh (structured/unstructured) for square plate domain.

Table 1. Error convergence and global effectivity (θ) obtained for RPI (MQ) and least square based displacement recovery techniques (linear triangular, L_2 norm).

Mesh Size (1/h)	FEM Error ($\times 10^{-3}$)	RPI (Mesh Free)		RPI (Mesh Dependent)		LS (Mesh Dependent)	
		Error ($\times 10^{-3}$)	Effectivity	Error ($\times 10^{-3}$)	Effectivity	Error ($\times 10^{-3}$)	Effectivity
1/4	5.365	3.084	0.63004	2.429	0.76209	3.791	0.70817
1/16	0.378	0.192	0.64754	0.140	0.83318	0.181	0.67755
1/32	0.0951	0.047	0.64615	0.034	0.84088	0.043	0.67375
Rate of Conv.	1.93939	2.01685		2.06494		2.15207	

Table 2. Error convergence and global effectivity (θ) obtained for RPI (MQ) and least square based displacement recovery techniques (quadratic triangular, L_2 norm).

Mesh Size (1/h)	FEM Error ($\times 10^{-3}$)	RPI (Mesh Free)		RPI (Mesh Dependent)		LS (Mesh Dependent)	
		Error ($\times 10^{-3}$)	Effectivity	Error ($\times 10^{-3}$)	Effectivity	Error ($\times 10^{-3}$)	Effectivity
1/4	0.24501	0.24755	1.30050	0.14612	0.95302	1.03015	4.24214
1/12	0.00842	0.00224	1.02195	0.00202	1.00023	0.01930	2.44485
1/24	0.00104	0.00014	1.01017	0.00014	1.00494	0.00132	1.58496
Rate of Conv.	3.04733	4.16168		3.86833		3.721499	

Table 3. Error convergence and global effectivity (θ) obtained for RPI (MQ) and least square based displacement recovery techniques (quadrilateral, L_2 norm).

Mesh Size (1/h)	FEM Error ($\times 10^{-3}$)	RPI (Mesh Free)		RPI (Mesh Dependent)		LS (Mesh Dependent)	
		Error ($\times 10^{-3}$)	Effectivity	Error ($\times 10^{-3}$)	Effectivity	Error ($\times 10^{-3}$)	Effectivity
1/4	2.032	2.280	1.64355	2.839	2.02455	1.840	1.83209
1/16	0.124	0.097	1.55565	0.176	2.28836	0.111	1.82651
1/32	0.031	0.028	1.51151	0.044	2.31024	0.028	1.82654
Rate of Conv.	2.01223	2.26171		2.00883		2.01729	

Table 4. Error convergence and global effectivity (θ) obtained for RPI with radial basis function types and least square based displacement recovery techniques (linear triangular, energy norm).

Mesh Size (1/h)	FEM Error ($\times 10^{-3}$)	RPI (Mesh Free)						RPI (Mesh Dependent)				LS (Mesh Dependent)	
		MQ		Exp		TSP		MQ		Exp			
		Error ($\times 10^{-3}$)	θ	Error ($\times 10^{-3}$)	θ	Error ($\times 10^{-3}$)	θ	Error ($\times 10^{-3}$)	θ	Error ($\times 10^{-3}$)	θ	Error ($\times 10^{-3}$)	θ
1/4	93.749	17.114	0.9469	58.476	0.8568	30.079	0.92276	26.233	0.8933	51.106	0.9096	58.478	0.9300
1/16	24.441	1.307	0.9931	7.385	0.9389	1.563	0.98496	1.586	1.0038	8.298	1.0860	4.462	0.9896
1/32	12.248	0.335	0.9975	2.684	0.9310	0.561	0.98924	0.425	1.0092	3.847	1.1195	1.158	0.9970
Rate of Conv.	0.97875	1.89163		1.48183		1.91524		1.98282		1.24389		1.89225	

Table 5. Error convergence and global effectivity (θ) obtained for RPI with radial basis function types and least square based displacement recovery techniques (quadratic triangular, energy norm).

Mesh Size (1/h)	FEM Error ($\times 10^{-3}$)	RPI (Mesh Free)						RPI (Mesh Dependent)				LS (Mesh Dependent)	
		MQ		Exp		TSP		MQ		Exp			
		Error ($\times 10^{-3}$)	θ	Error ($\times 10^{-3}$)	θ	Error ($\times 10^{-3}$)	θ	Error ($\times 10^{-3}$)	θ	Error ($\times 10^{-3}$)	θ	Error ($\times 10^{-3}$)	θ
1/4	13.168	7.493	1.1596	35.032	2.8637	5.782	1.10655	3.941	1.0294	4.445	1.0548	12.258	1.2556
1/12	1.515	0.184	1.0135	0.560	1.0853	0.199	1.01836	0.174	1.0093	0.257	1.0162	0.529	1.0405
1/24	0.380	0.025	1.0057	0.0678	1.0275	0.023	1.00292	0.026	1.0053	0.0613	1.0116	0.070	1.0127
Rate of Conv.	1.97848	3.1910		3.48633		3.09017		2.76963		2.39122		2.88449	

Table 6. Error convergence and global effectivity (θ) obtained for RPI with radial basis function types and least square based displacement recovery techniques (quadrilateral, energy norm).

Mesh Size (1/h)	FEM Error ($\times 10^{-3}$)	RPI (Mesh Free)						RPI (Mesh Dependent)				LS (Mesh Dependent)	
		MQ		Exp		TSP		MQ		Exp			
		Error ($\times 10^{-3}$)	θ	Error ($\times 10^{-3}$)	θ	Error ($\times 10^{-3}$)	θ	Error ($\times 10^{-3}$)	θ	Error ($\times 10^{-3}$)	θ	Error ($\times 10^{-3}$)	θ
1/4	60.262	13.249	1.0541	52.222	0.8173	27.595	1.0121	23.053	1.0263	46.792	0.8560	13.667	1.0810
1/16	15.015	0.797	0.9967	7.272	1.0063	1.272	0.9805	1.294	1.0130	6.593	0.9669	0.813	1.0051
1/32	7.506	0.201	0.9967	2.536	1.0191	0.622	0.9615	0.323	1.0164	2.303	0.9782	0.201	1.0013
Rate of Conv.	1.00169	2.01497		1.45472		1.82359		2.05275		1.44822		2.02723	

6.1.1. Mesh Free and Mesh Dependent Displacement Recovery Techniques

The finite element errors quantified in terms of L_2 norms and effectivity of error estimation, using mesh free radial point interpolation (RPI) approach and mesh dependent least square (LS) and RPI approach with triangular (3/6 Nodes) and quadrilateral (4 Nodes) mesh for displacements recovery, are presented in Tables 1–3. The RPI approach considers the multi-quadratics radial basis function for interpolation purpose, and structured mesh are employed in the analysis.

6.1.2. RPI Recovery Technique and Radial Basis Function Type

The characteristics of error estimation using RPI-based recovery technique are obtained considering Multi-quadrics (MQ), Gaussian or Exponential (Exp), and Thin plate splint (TSP) radial basis functions. Tables 1–3 present Multi-quadrics (MQ) RBF-based RPI recovery analysis results wherein errors are quantified in L_2 norms. The finite element errors in energy norms and effectivity of error estimation, using radial point interpolation (RPI) approach considering Multi-quadrics (MQ), Gaussian (Exponential), and Thin plate splint (TSP) RBFs, with triangular (3/6 Nodes) and quadrilateral (4 Nodes) structured mesh are tabulated in Tables 4–6.

6.1.3. RPI Recovery Technique and Patch Configuration

In almost all adaptive finite element analyses, unstructured meshes are employed. Therefore, it is of interest to test the robustness of RPI-based displacement recovery technique also in unstructured meshes. The finite element errors quantified in terms of L_2 norm and effectivity of error estimation, using mesh free radial point interpolation (RPI) approach and mesh dependent RPI approach with multi-quadratic radial basis function (MQ) and least square (LS) approach considering circular and rectangular mesh free node zones of triangular (3/6 Nodes) and quadrilateral (4 Nodes) unstructured mesh for displacements recovery are presented in Tables 7–9. The computation results error estimation in energy norm with circular and rectangular mesh free node zones of quadrilateral (4 Nodes) unstructured mesh is shown in Table 10.

Table 7. Error convergence and global effectivity (θ) obtained for RPI (MQ) and least square based displacement recovery techniques (linear triangular, L_2 norm).

Mesh Size		FEM (Exact Error) ($\times 10^{-3}$)	RPI (MQ) Recovery						LS Recovery	
			Circular Mesh Free Patch		Rectangular Mesh Free Patch		Mesh Dependent Patch		Mesh Dependent Patch	
Elem.	DOF		Error ($\times 10^{-3}$)	θ	Error ($\times 10^{-3}$)	θ	Error ($\times 10^{-3}$)	θ	Error ($\times 10^{-3}$)	θ
103	136	1.534	0.630	0.83865	0.635	0.82329	0.603	0.83264	0.915	0.88585
470	530	0.282	0.117	0.93473	0.116	0.91067	0.115	0.97121	0.141	0.93646
1887	2004	0.070	0.029	0.94503	0.029	0.91226	0.028	0.99068	0.029	0.91340

Table 8. Error convergence and global effectivity (θ) obtained for RPI (MQ) and least square based displacement recovery techniques (quadratic triangular, L_2 norm).

Mesh Size		FEM (Exact Error) ($\times 10^{-3}$)	RPI (MQ) Recovery						LS Recovery	
			Circular Mesh Free Patch		Rectangular Mesh Free Patch		Mesh Dependent Patch		Mesh Dependent Patch	
Elem.	DOF		Error ($\times 10^{-3}$)	θ	Error ($\times 10^{-3}$)	θ	Error ($\times 10^{-3}$)	θ	Error ($\times 10^{-3}$)	θ
103	476	0.056	0.039	0.95236	0.034	0.94796	0.032	0.87951	0.121	2.38461
470	1998	0.247	0.0028	0.96288	0.0025	0.96605	0.0025	0.90108	0.0073	1.66566
1887	7780	0.059	0.00033	0.98617	0.00030	0.98079	0.00031	0.93046	0.00054	1.27775

Table 9. Error convergence and global effectivity (θ) obtained for RPI (MQ) and least square based displacement recovery techniques (quadrilateral, L_2 norm).

Mesh Size		FEM (Exact Error) ($\times 10^{-3}$)	RPI (MQ) Recovery						LS Recovery	
			Circular Mesh Free Patch		Rectangular Mesh Free Patch		Mesh Dependent Patch		Mesh Dependent Patch	
Elem.	DOF		Error ($\times 10^{-3}$)	θ	Error ($\times 10^{-3}$)	θ	Error ($\times 10^{-3}$)	θ	Error ($\times 10^{-3}$)	θ
186	432	0.356	0.303	1.43564	0.298	1.43444	0.299	1.48273	0.249	1.40829
593	1282	0.133	0.094	1.38343	0.092	1.36857	0.093	1.38133	0.075	1.28740
1333	2806	0.054	0.040	1.37238	0.040	1.36711	0.041	1.38847	0.034	1.30001

Table 10. Error convergence and global effectivity (θ) obtained for RPI (MQ) and least square based displacement recovery techniques (quadrilateral energy norm).

Mesh Size		FEM (Exact Error) ($\times 10^{-3}$)	RPI (MQ) Recovery						LS Recovery	
			Circular Mesh Free Patch		Rectangular Mesh Free Patch		Mesh Dependent Patch		Mesh Dependent Patch	
Elem.	DOF		Error ($\times 10^{-3}$)	θ	Error ($\times 10^{-3}$)	θ	Error ($\times 10^{-3}$)	θ	Error ($\times 10^{-3}$)	θ
186	432	22.764	8.269	1.04925	8.349	1.04267	8.579	1.08869	6.305	1.06260
593	1282	13.917	3.859	1.07186	4.348	1.05353	4.089	1.08202	1.821	1.01123
1813	3790	7.994	2.410	1.05454	2.452	1.03180	2.635	1.08825	1.011	1.00801

6.2. Square Plate with Opening Problem

A problem involving a square portion from an infinite elastic plate having a circular opening with a radius (a) of 1 unit is also analyzed to demonstrate the effectiveness of RPI-based displacement recovery technique in stress concentration conditions. The one-quarter of the plate domain is modeled because of the symmetry of the plate. The plate domain with an opening is discretized with triangular/quadrilateral elements, as shown in Figure 5. Along the symmetry line, the normal displacement component and shear stress are zero. A unit in-plane traction is applied in the x-direction. The close form solution of stress field for an infinite plate with opening is given in Equations (38)–(40) [4].

$$\sigma_x = \sigma_\infty \{1 - [(a^2/r^2)(1.5\cos 2\theta + \cos 4\theta)] + (1.5\, a^4/r^4 \cos 4\theta) \quad (38)$$

$$\sigma_y = \sigma_\infty \{0 - [(a^2/r^2)(0.5\cos 2\theta - \cos 4\theta)] + (1.5\, a^4/r^4 \cos 4\theta) \quad (39)$$

$$\sigma_{xy} = \sigma_\infty \{0 - [(a^2/r^2)(0.5\sin 2\theta + \sin 4\theta)] + (1.5\, a^4/r^4 \sin 4\theta) \quad (40)$$

where $r^2 = y^2 + x^2$ and σ_∞ is the uniaxial traction applied at infinity.

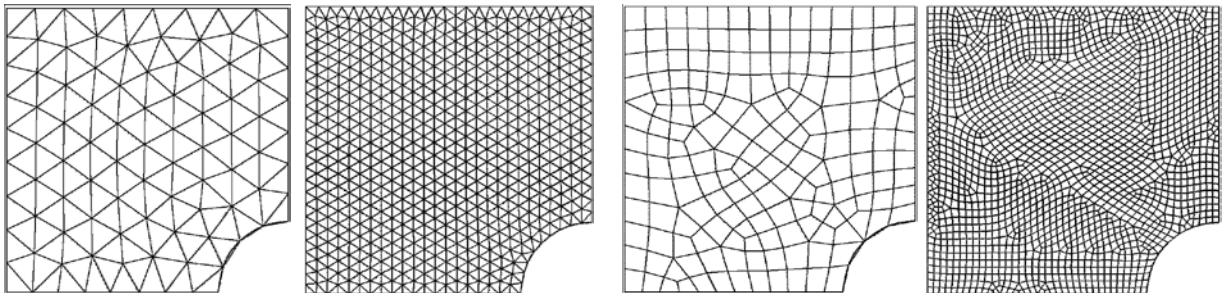

(**a**) Triangular Elements (**b**) Quadrilateral Elements

Figure 5. Triangular/quadrilateral elements mesh for plate with opening domain.

The finite element analysis of the problem is carried out incorporating mesh dependent and mesh independent RPI-based displacement error recovery techniques. The error estimation obtained with RPI recovery techniques is compared with least square displacement recovery techniques. The analyses results are also obtained employing Zienkiewicz-Zhu (ZZ) recovery techniques presented in the literature [18] for comparison with RPI-based error recovery techniques. The recovery results are compared in terms of convergence errors and global effectivity. The computational results obtained are tabulated in Tables 11–13.

Table 11. Error convergence and global effectivity (θ) for plate problem with hole using RPI (MQ) with various mesh free node zones and least square based recovery techniques (linear triangular, energy norm).

Mesh Size		FEM (Exact Error) ($\times 10^{-3}$)	RPI (MQ) Recovery						LS Recovery (Mesh Dependent)			
			Circular Zone		Rectangular Zone		Mesh Dependent Patch		Element Patch		Node Patch (ZZ) [18]	
Elem.	DOF		Error ($\times 10^{-3}$)	θ	Error ($\times 10^{-3}$)	θ	Error ($\times 10^{-3}$)	θ	Error ($\times 10^{-3}$)	θ	Error ($\times 10^{-3}$)	θ
155	194	12.905	7.636	0.78552	7.768	0.78485	8.253	0.73122	11.206	0.80541	13.231	1.01807
548	618	8.504	4.442	0.91893	4.402	0.94074	4. 814	0.89851	5.495	0.90648	7.913	1.12593
1585	1700	5.171	2.251	0.93567	2.450	0.96781	2.244	0.93447	2.572	0.90042	4.672	1.14923

Table 12. Error convergence and global effectivity (θ) for plate problem with hole using exponential (Exp) and thin plate splint (TPS) radial basis function-based RPI error recovery techniques (linear triangular, energy norm).

Mesh Size		FEM Error ($\times 10^{-3}$)	RPI (Exp)				RPI (TPS)			
			Mesh Free		Mesh Dependent		Mesh Free		Mesh Dependent	
Elem.	DOF		Error ($\times 10^{-3}$)	θ	Error ($\times 10^{-3}$)	θ	Error ($\times 10^{-3}$)	θ	Error ($\times 10^{-3}$)	θ
155	194	12.905	11.739	1.06061	10.845	1.20390	8.256	0.79118	13.611	0.92793
548	618	8.504	7.297	0.89907	6.587	1.29955	4.653	0.91835	5.926	0.88131
1585	1700	5.171	8.108	1.55389	4.783	0.95750	2.157	0.92439	4.095	0.95173

Table 13. Error convergence and global effectivity (θ) for plate problem with hole using RPI (MQ) and least square based recovery techniques (quadrilateral, energy norm).

Mesh Size		FEM (Exact Error) ($\times 10^{-3}$)	RPI (MQ) Recovery				LS Recovery (Mesh Dependent)			
			Circular Mesh free		Mesh Dependent Patch		Element Patch		Node Patch (ZZ) [18]	
Elem.	DOF		Error ($\times 10^{-3}$)	θ	Error ($\times 10^{-3}$)	θ	Error ($\times 10^{-3}$)	θ	Error ($\times 10^{-3}$)	θ
179	414	8.085	5.377	1.01183	5.377	0.92632	7.286	0.94018	9.262	1.40135
578	1254	4.291	2.196	0.94201	2.420	0.94167	2.949	0.99933	2.404	0.89920
1842	3854	2.882	1.604	0.94551	1.696	0.89699	1.703	0.94552	1646	0.91160

The efficiency and reliability of recovery technique under different mesh free and mesh dependent interpolation schemes is demonstrated through finite element analysis in an adaptive environment. The initial meshes are adaptively refined to bring the solution error below the target error limit. Table 14 shows the global error, number of elements, and degree of freedom DOF in refined meshes at prescribed error limit of 2% using the RPI error recovery employing Multi-quadrics (MQ), Gaussian (GS), and thin plate splint radial basis functions, circular and rectangular support domain shapes. The adaptively refined meshes at 2% target error using mesh free and mesh dependent RPIM, and mesh dependent least square based error estimation employing different radial basis function and node zone shapes are displayed in Figures 6–8.

Table 14. Global errors using various recovery-based finite element analysis and number of elements (N) with DOF in adaptively improved meshes for 2% target error.

Recovery Type	Linear Triangle (Uniform Mesh Having 548 Elements and 618 DOF)				Linear Quadrilateral (Uniform Mesh Having 179 Elements and 414 DOF)			
	FEM Error	Proj. Error	Adaptive Mesh (2%) N	Adaptive Mesh (2%) DOF	FEM Error	Proj. Error	Adaptive Mesh (2%) N	Adaptive Mesh (2%) DOF
LS (Mesh Dependent)	6.84	6.22	781	866	6.50	6.14	1444	3032
LS (Mesh Dependent-ZZ)	6.84	7.66	922	1012	6.50	9.25	1816	3784
RPI (Mesh Free-MQ-Cir.)	6.84	6.32	1004	1098	6.50	6.42	1468	3082
RPI (Mesh Free-MQ-Rec.)	6.84	6.47	1050	1140	6.50	5.96	1422	2990
RPI (Mesh Dependent-MQ)	6.84	6.18	1175	1274	6.50	6.39	1452	3028
RPI (Mesh Free-Exp.-Cir.)	6.84	6.14	417	486				
RPI (Mesh Dependent-Exp.)	6.84	8.90	1155	1242				
RPI (Mesh Free-TSP-Cir.)	6.84	6.31	945	1038				
RPI (Mesh Dependent-TSP)	6.84	6.06	1100	1200				

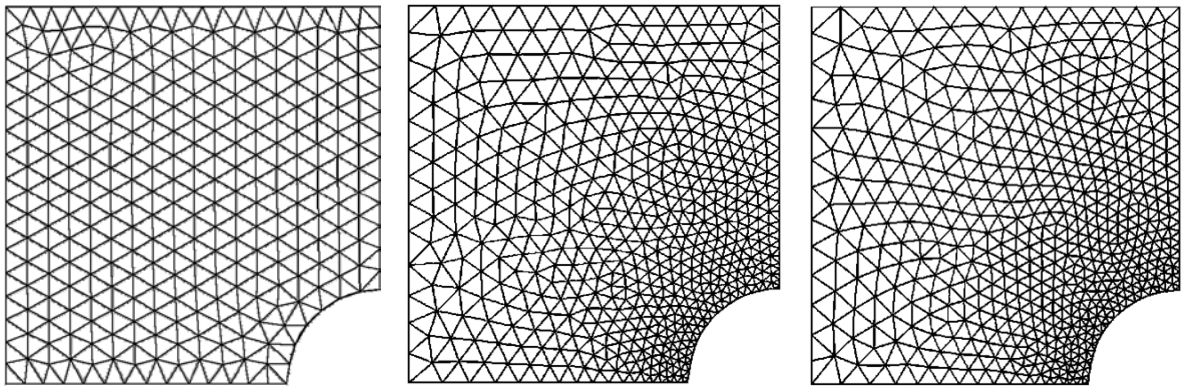

(**a**) Initial Mesh (**b**) RPI-MQ (MF-Cir) (**c**) RPI-MQ (MF-rect)

Figure 6. *Cont.*

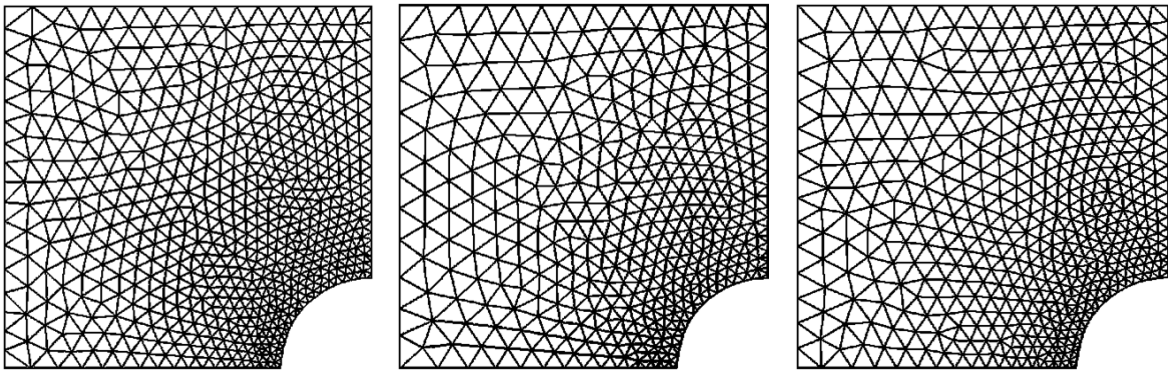

(**d**) RPI-MQ (MD) (**e**) Least Square (MD) (**f**) Least Square-ZZ (MD)

Figure 6. Adaptively improved mesh in elastic plate with opening using mesh free (MF) RPI having different node zone shape and least square error recovery analysis (initial triangular mesh elements = 548, 2% target error).

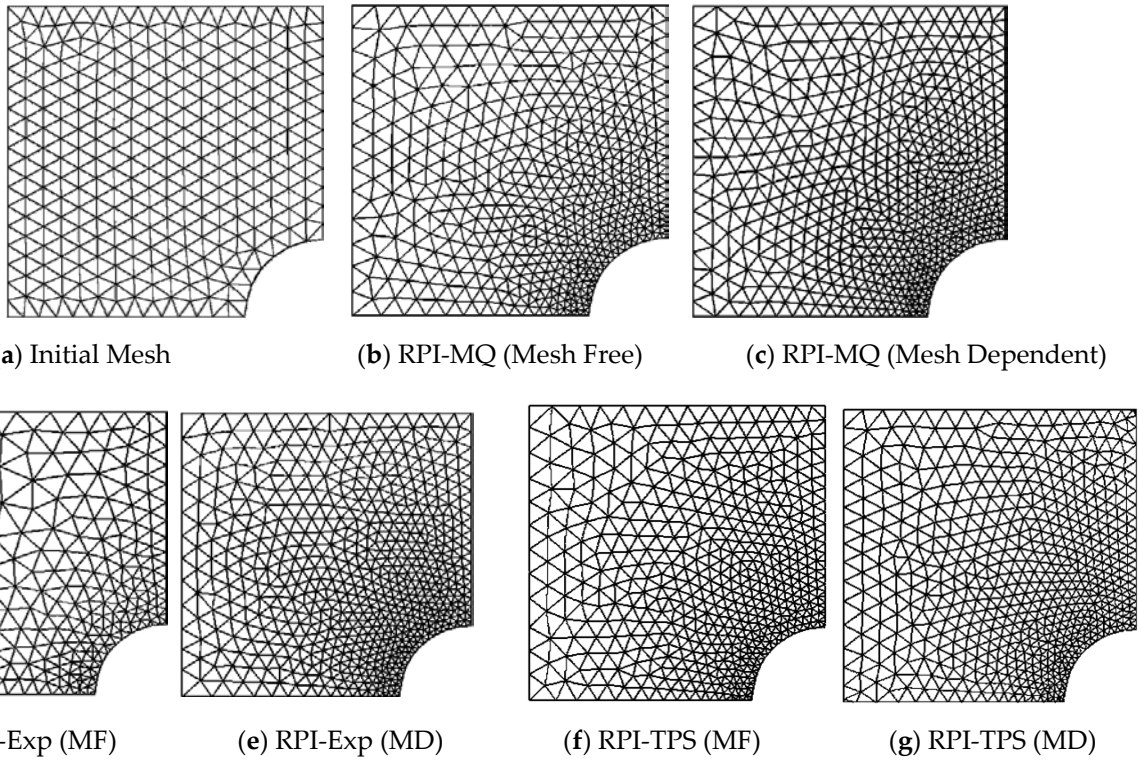

(**a**) Initial Mesh (**b**) RPI-MQ (Mesh Free) (**c**) RPI-MQ (Mesh Dependent)

(**d**) RPI-Exp (MF) (**e**) RPI-Exp (MD) (**f**) RPI-TPS (MF) (**g**) RPI-TPS (MD)

Figure 7. Adaptively improved mesh in elastic plate with opening using meshfree (MF) RPI, mesh dependent (MD) RPI having different radial basis function (initial triangular mesh elements = 548, 2% target error).

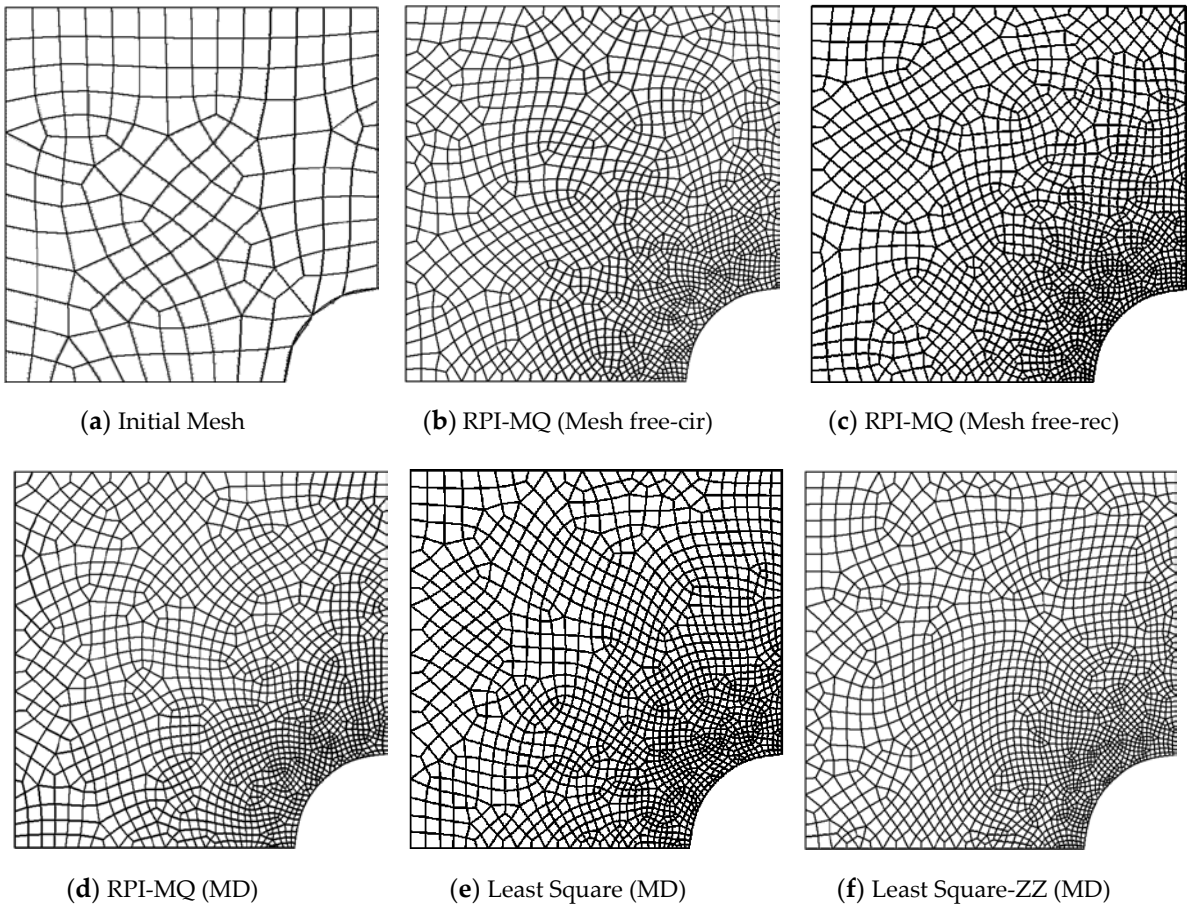

(**a**) Initial Mesh (**b**) RPI-MQ (Mesh free-cir) (**c**) RPI-MQ (Mesh free-rec)

(**d**) RPI-MQ (MD) (**e**) Least Square (MD) (**f**) Least Square-ZZ (MD)

Figure 8. Adaptively improved mesh in elastic plate with opening using mesh free RPI, mesh dependent RPI and least square error recovery analysis (initial quadrilateral mesh elements = 179, 2% target error).

7. Discussion

The reliability and effectiveness of RPIM-based displacement error recovery techniques in a mesh free environment is studied. The comparison of mesh free RPIM-based displacement error recovery techniques with mesh dependent RPIM and least square based recovery techniques is also carried out. The performance of Zienkiewicz-Zhu ZZ recovery techniques [18] is also compared with RPI-based error recovery techniques. The RPI technique uses the nodal values in the local support domain to interpolate the field variable or field variable derivatives. The elastic square plate problems under the action of body forces and unit in-plane traction are analyzed using finite element method coupled with RPI-based error recovery considering mesh free circular/rectangular support domains and mesh dependent node patches. The RPIM-based displacement error recovery techniques employ Multi-Quadrics (MQ) and Gaussian or Exponential (Exp) radial basis functions. The problem domain is discretized using linear/quadratic triangular and quadrilateral shape elements. The error analysis is further utilized for adaptive improvement of domain mesh. The quality of discretization error obtained using recovery techniques is compared in terms of error convergence characteristics, error effectivity, and adaptively refined element meshes with specified target error. The errors are computed in L_2 norm as well as in energy norm. The computation results obtained with increasing fineness order, radial basis functions, mesh free node zones shapes, and error norms, for elastic plate problem under the action of body forces, are depicted in Tables 1–10. The results of error convergence rate, effectivity index, and adaptive refined meshes for 2% target accuracy obtained for an infinite plate with an opening are given in Tables 11–14 and Figures 6–8.

The finite element analysis results of benchmark problems using the mesh free RPI, mesh-based RPI and least square recovery techniques with increasing order of mesh fineness, show that the RPI recovery techniques predict lower order of error and higher convergence rate of the error, than that of the finite element solution and mesh dependent least square based recovery techniques with better effectivity. The mesh free RPI recovery techniques predict lower order of error with higher convergence rate than that of the mesh dependent RPI error recovery techniques. It may be due to the possibility of less accurate recovery for boundary nodes in mesh dependent recovery technique since a smaller number of nodes are available. Such difficulty does not arise with mesh free RPI-based displacement recovery technique. The effect of choice of element for domain discretization on error convergence of RPI recovery techniques and least square recovery techniques is clearly observed in the recovery analysis results. The performance of linear quadrilateral elements discretization used in mesh free and mesh dependent RPI-based recovery techniques and mesh dependent least square recovery techniques is found better than the linear and quadratic triangular element discretization as the higher convergence rate, lesser order of error and effectivity index, in general, near to one. From the error quantified in energy and L_2 norms, it is found that it is better to employ the L_2 norm for error representation for higher order elements as effectivity converge to nearly one and with a higher convergence rate as compared to lower order element. The convergence rate for linear triangular, quadratic triangular, and linear quadrilateral structured mesh, for finite element solution of plate problem using mesh free RPI (MQ), mesh-based RPI (MQ), and least square recovery techniques, in L_2 norm are obtained as (1.93939, 2.01685, 2.06494, 2.15207), (3.04733, 4.16168, 3.86833, 3.721499), and (2.01223, 2.26171, 2.00883, 2.01729), respectively. The corresponding error convergence rate for 3/6/4 node elements in energy norm are found as (0.97875, 1.89163, 1.98282, 1.89225), (1.97848, 3.19100, 2.769632, 2.88449), and (1.00169, 2.01497, 2.05275, 2.02723), respectively. There is a pronounced effect of the kind of radial basis function on the RPI recovery-based error estimation. It is found that the characteristics of error recovery considering the Multi-Quadrics radial basis function are much superior to the Gaussian or Exponential radial basis functions in both mesh free and mesh dependent RPI recovery analysis. The convergence rate with Multi-Quadrics, Exponential, and Thin plate splint radial basis functions in mesh free RPI recovery analysis for 3/6/4 node elements in energy norm are, respectively, obtained as (1.89163, 1.48183, 1.91524), (3.19100, 3.48633, 3.09017), and (2.01497, 1.45472, 1.82359). The convergence rate with Multi-Quadrics and Exponential RBF in mesh dependent RPI recovery analysis for 3/6/4 node elements in energy norm are respectively obtained as (1.98282, 1.24389), (2.769632, 2.39122), and (2.05275, 1.44822). The shape of the support domains, i.e., circular, or rectangular, has no significant influence on the RPI-based error estimation provided that enough nodes are enclosed in the support domain. Similar results are also confirmed from the mesh free and mesh dependent RPI-based displacement error recovery analysis of an infinite plate with an opening as shown in Tables 11–14, giving rate of convergence and effectivity index. It implies from the discussion that the type of element, the norm used to quantify the errors, and radial basis functions influence considerably on the RPI-based displacement error recovery of finite element solution.

The performance of error estimation using mesh free and mesh dependent RPI displacement error recovery technique and least square recovery technique is also demonstrated in terms of adaptively improved meshes with target error limits. The adaptive finite element results for the plate problem with an opening are presented in Table 14 and Figures 6–8 at a prescribed error limit of 2% for different radial basis functions and node zones. The adaptively improved meshes indicate the error distribution pattern in the domain as the meshes become finer in areas of high errors to obtain a uniform accuracy throughout the domain. It is concluded that the RPI-based mesh free error estimation technique can be used to predict the zones of high computational errors. The number of elements required to achieve target accuracy, in general, is smaller in RPI error estimations as compared to mesh dependent RPI and mesh dependent least square error

estimation for both triangular and quadrilateral elements discretization. The characteristics of adaptive mesh obtained using the mesh free RPI-based error recovery technique using Multi-Quadrics radial basis function are superior to mesh free RPI-based error recovery technique using Gaussian and thin plate splint radial basis function. It is also observed that the performance of RPI-based displacement recovery technique is superior to ZZ stress recovery technique [18]. The numerical results show that the mesh free RPI-based displacement recovery technique is more effective and achieves target accuracy in adaptive analysis with a smaller number of elements as compared to mesh dependent RPI and mesh dependent least square. It is also concluded that the proposed mesh free recovery technique may prove to be most suitable for error recovery and adaptive analysis of problems dealing with large domain changes and domain discontinuities.

8. Present Study Limitations and Future Research Work

The accuracy and the performance of the RPIM techniques depend on suitable and optimized values of shape parameters of radial basis functions. Therefore, the performance is limited to the shape parameters taken in the study. The present study is limited to the performance of mesh free RPI-based error recovery technique for two-dimensional linear elastic problems. The study could be extended the application of mesh free RPI-based error recovery to incompressible elastic problems. The study could also be conducted by applying mesh free recovery techniques to large deformation problems or plastic problems. The different adaptive procedures could also be tested using RPI-based error estimators.

9. Conclusions

The present study is a contribution towards the development of a reliable and cost-effective displacement recovery-based error estimation technique using RPIM in mesh free and mesh dependent environments. The study considers three radial basis functions, namely Multi-Quadrics, Gaussian, or Exponential and thin plate splint RBF, and circular and rectangular support domain shape for error recovery analysis. Finite element analysis on test examples is carried out using linear and higher order triangular and quadrilateral elements for discretization and employing RPI-based recovery technique. The finite element solution errors in energy/L_2 norms are calculated directly from the recovered displacement. The characteristics of RPI-based error recovery with different radial basis function is compared in terms of error convergence properties, effectivity, and adaptively refined meshes. It is found from the results that the L_2 norm for error representation is better for higher order elements, while the energy norm is equally good for all types of elements. It is concluded that the multi-quadrics radial basis function found to perform better in RPI-based error recovery of finite element solution and radial basis functions shape parameters can be optimized for better performance. It is verified that radial basis functions with their shape parameters, choice of elements for discretization, and norm used to quantify the errors influence considerably on the RPI-based displacement error recovery of finite element solution. The study concludes that mesh free RPI-based displacement error recovery technique with multi-quadrics radial basis function is more effective and efficient than the mesh dependent least square based displacement recovery technique. The numerical results show that the mesh free RPI-based displacement recovery technique is more effective and achieves target accuracy in adaptive analysis with a smaller number of elements as compared to mesh dependent RPI and mesh dependent least square. The study concludes that mesh free RPI-based displacement recovery technique is more effective and efficient, and the number of elements required to achieve target accuracy is smaller in RPI error estimations as compared to mesh dependent RPI and mesh dependent least square error estimation. It is also concluded that the proposed mesh free recovery technique may prove to be most suitable for error recovery and adaptive analysis of problems dealing with large domain changes and domain discontinuities.

Author Contributions: Conceptualization, M.A. and D.S.; methodology, M.A.; software, D.S.; validation, S.A. and M.A.A.; formal analysis, M.A. and S.A.; investigation, M.A.; resources, S.A.; data

curation, M.A.A.; writing—original draft preparation, M.A.; writing—review and editing, S.A. and M.A.A.; visualization, S.A.; supervision, D.S.; project administration, M.A.A.; funding acquisition, M.A. All authors have read and agreed to the published version of the manuscript.

Funding: The authors extend their appreciation to the Deanship of Scientific Research at King Khalid University for funding this work through General Research Project under grant number [R.G.P2/73/41].

Institutional Review Board Statement: Not Applicable.

Informed Consent Statement: Not Applicable.

Data Availability Statement: Not Applicable.

Acknowledgments: The authors acknowledge to the Dean, Faculty of Engineering for his valuable support and help.

Conflicts of Interest: The authors declare no conflict of interest. The funders had no role in the design of the study; in the collection, analyses, or interpretation of data; in the writing of the manuscript, or in the decision to publish the results.

References

1. Taus, M.; Rodin, G.J.; Hughes, T.J.R.; Scott, M.A. Isogeometric boundary element methods and patch tests for linear elastic problems: Formulation, numerical integration, and applications. *Comput. Methods Appl. Mech. Eng.* **2019**, *357*, 112591. [CrossRef]
2. Cen, S.; Wu, C.J.; Li, Z.; Shang, Y.; Li, C. Some advances in high-performance finite element methods. *Eng. Comput.* **2019**, *36*, 2811–2834. [CrossRef]
3. Grosse, I.; Katragadda, P.; Benoit, J. An adaptive accuracy-based a posteriori error estimator. *Finite Elem. Anal. Des.* **1992**, *12*, 75–90. [CrossRef]
4. Zienkiewicz, O.C.; Zhu, J.Z. The superconvergent patch recovery anda posteriori error estimates. Part 1: The recovery technique. *Int. J. Numer. Methods Eng.* **1992**, *33*, 1331–1364. [CrossRef]
5. Niu, Q.; Shephard, M.S. Super-convergent Extraction Techniques for Finite Element Analysis. *Int. J. Num. Meth. Eng.* **1993**, *36*, 811–836. [CrossRef]
6. Li, X.; Wiberg, N.-E. A posteriori error estimate by element patch post-processing, adaptive analysis in energy and L2 norms. *Comput. Struct.* **1994**, *53*, 907–919. [CrossRef]
7. Ubertini, F. Patch recovery based on complementary energy. *Int. J. Numer. Methods Eng.* **2004**, *59*, 1501–1538. [CrossRef]
8. Ullah, Z.; Coombs, W.; Augarde, C. An adaptive finite element/meshless coupled method based on local maximum entropy shape functions for linear and nonlinear problems. *Comput. Methods Appl. Mech. Eng.* **2013**, *267*, 111–132. [CrossRef]
9. Chung, H.-J.; Belytschko, T. An error estimate in the EFG method. *Comput. Mech.* **1998**, *21*, 91–100. [CrossRef]
10. Yang, C.S.; Lee, F.B.; Kao, S.-P.; Hung, P.-S. Twelve different interpolation methods: A case study of Surfer 8.0. In Proceedings of the XXth ISPRS Congress, Istanbul, Turkey, 12–23 July 2004; pp. 778–785.
11. Chen, X.L.; Liu, G.R.; Lim, S.P. The effects of the enforcement of compatibility in the radial point interpolation method for analyzing mindlin plates. In *Advances in Meshfree and X-FEM Methods*; World Scientific: Singapore, 2002; pp. 84–89.
12. Liu, G.R.; Zhang, G.Y.; Dai, K.Y.; Wang, Y.Y.; Zhong, Z.H.; Li, G.Y.; Han, X. A linearly conforming point interpolation method (lc-pim) for 2d solid mechanics problems. *Int. J. Comput. Methods* **2005**, *2*, 645–665. [CrossRef]
13. Liu, G.R.; Zhang, G.Y. A novel scheme of strain-constructed point interpolation method for static and dynamic mechanics problems. *Int. J. Appl. Mech.* **2009**, *1*, 233–258. [CrossRef]
14. Mirzaei, D. Analysis of moving least squares approximation revisited. *J. Comput. Appl. Math.* **2015**, *282*, 237–250. [CrossRef]
15. Hamrani, A.; Belaidi, I.; Monteiro, E.; Lorong, P. On the Factors Affecting the Accuracy and Robustness of Smoothed-Radial Point Interpolation Method. *Adv. Appl. Math. Mech.* **2016**, *9*, 43–72. [CrossRef]
16. Zhang, G.; Wang, Y.; Jiang, Y.; Jiang, Y.; Zong, Z. A combination of singular cell-based smoothed radial point inter-polation method and FEM in solving fracture problem. *Int. J. Comput. Methods* **2018**, *15*, 1850079. [CrossRef]
17. Ahmed, M.; Singh, D.; Desmukh, M.N. Interpolation type stress recovery technique based error estimator for elasticity problems. *Mechanika* **2018**, *24*, 672–679. [CrossRef]
18. Ahmed, M.; El Ouni, M.H.; Singh, D.; Kahla, N.B. A parametric study of meshfree interpolation based recovery techniques in finite element elastic analysis. *CMES Comput. Model. Engg. Sci.* **2019**, *121*, 687–786.
19. Ahmed, M. A Comparative study of mesh-free radial point interpolation method and moving least squares method-based error estimation in elastic finite element analysis. *Arab. J. Sci. Eng.* **2020**, *45*, 3541–3557. [CrossRef]
20. Gong, J.; Zou, D.; Kong, X.; Qu, Y.; Zhou, Y. A Non-Matching Nodes Interface Model with Radial Interpolation Function for Simulating 2D Soil–Structure Interface Behaviors. *Int. J. Comput. Methods* **2020**, *18*, 2050023. [CrossRef]
21. Liu, G.R.; Gu, Y.T. A local radial point interpolation method (LR-PIM) for free vibration analyses of 2-D solids. *J. Sound Vib.* **2001**, *246*, 29–46. [CrossRef]

22. Wang, J.; Liu, G. On the optimal shape parameters of radial basis functions used for 2-D meshless methods. *Comput. Methods Appl. Mech. Eng.* **2002**, *191*, 2611–2630. [CrossRef]
23. Wang, J.; Liu, G.R. A point interpolation meshless method based on radial basis functions. *Int. J. Numer. Methods Eng.* **2002**, *54*, 1623–1648. [CrossRef]
24. Zienkiewicz, O.C.; Zhu, J.Z. A simple error estimator and adaptive procedure for practical engineering analysis. *Int. J. Numer. Methods Eng.* **1987**, *24*, 337–357. [CrossRef]